Verification and validation of MoodyMarine: A free simulation tool for modelling moored MRE devices

Johannes Palm and Claes Eskilsson

Abstract—**This work presents the verification and validation of the freely available simulation tool MoodyMarine, developed to help meet some of the demands for early stage development of MRE devices. MoodyMarine extends the previously released mooring module MoodyCore (Discontinuous Galerkin Finite Elements) with linear radiation-diffraction bodies, integrated pre-processing workflows and a graphical user interface. It is a C++ implementation of finite element mooring dynamics and Cummins equations for floating bodies with weak nonlinear corrections. A newly developed nonlinear Froude-Krylov implementation is verified in the paper, and MoodyMarine is compared to CFD simulations for two complex structures: a slack-moored floating offshore wind turbine and a self-reacting point-absorber with hybrid mooring.**

Index Terms—**Linear potential flow, wave-to-wire, mooring dynamics, graphical user interface**

I. Introduction

RELIABLE and affordable numerical tools are required to evaluate design alternatives along the development path of a Marine Renewable Energy (MRE) device. The hydrodynamic evaluation is typically made with time domain radiation-diffraction models based on linear potential flow (LPF), but simulations of higher fidelity are also needed to ascertain validity in numerical predictions. Many LPF models are commercial [1], [2], whereas some have been developed by the research community and are released as free tools [3]–[5].

The present work has dual purpose. First, this paper marks the first release of MoodyMarine, a freely available time-domain simulation tool for floating marine installations. MoodyMarine does not rely on underlying commercial software and comes with an easy to use graphical user interface (GUI). Secondly, the paper aims to describe and validate an implementation of Cummins equation and its mesh-based Froude-Krylov solver (nonlinear Froude-Krylov correction) into MoodyMarine.

Support for this work was given by the Swedish Energy Agency through Grant No. 50196-1.

J. Palm is with Sigma Energy & Marine AB, Ekelundsgatan 1-3, SE-411 18 Gothenburg, Sweden (e-mail: johannes.palm@sigma.se).

C. Eskilsson is with the Hydrodynamic Research Unit, RISE – Research Institutes of Sweden, Box 857, SE-501 15 Borås, Sweden (e-mail: claes.eskilsson@ri.se); and the Department of the Built Environment, Aalborg University, Thomas Manns Vej 23, DK-9220 Aalborg Ø, Denmark (e-mail: claese@build.aau.dk).

Digital Object Identifier:
https://doi.org/10.36688/ewtec-2023-paper-317

The paper provides an overview of available features and modules in MoodyMarine (Section II), a description of the main governing equations (Section III), and a verification of newly developed features such as the non-linear Froude-Krylov (nlfk) force correction to Cummins equation (Section IV). Further, validations of the linearized hydrodynamics model are presented in Section V for the cases of (i) a moored floating offshore wind turbine (FOWT) are compared with a high-fidelity CFD simulation; and (ii) an operational WEC with hybrid mooring system.

II. Model description

This paper introduces MoodyMarine, a freely available time-domain solver for marine installations. MoodyMarine hosts a GUI for MoodyCore, see Fig. 1, as well as a set of utilities for setting up the workflow. MoodyMarine is implemented as a javascript react-application [6] using threejs [7] for 3D visualisation (all 3D figures in this paper has been generated using MoodyMarine). It has been compiled as a desktop app for Windows, Linux and Mac using Electron.js [8]. MoodyMarine is available from **`www.moodymarine.se`** .

The underlying C++ computational implementation of the software is a mooring module named MoodyCore, with time-domain modelling of mooring lines and floating bodies in waves that has been developed since 2016, see [9]–[12]. The solver is documented in the MoodyCore v3.0 Manual [13], and is typically operated from the command line. The module API has over the years been used to model dynamic moorings in external hydrodynamic code packages such as OpenFOAM [14], [15] and WEC-Sim [16].

Of note is also that an interface to the open-source radiation-diffraction problem solver Nemoh [17], is provided as an add-on. The hydrostatics are however computed internally in MoodyCore. This has the benefit of using a nonlinear geometry during the static solver stage, to find the moored equilibrium positions prior to running the pre-processor (Nemoh). Such a workflow is outlined below:

1) Define environmental properties (water level, ground, waves...)
2) Define floating body properties with mass and mesh file (stl, wamit or nemoh format)
3) Assign mooring system.
4) Use the static solver to find the moored equilibrium position.

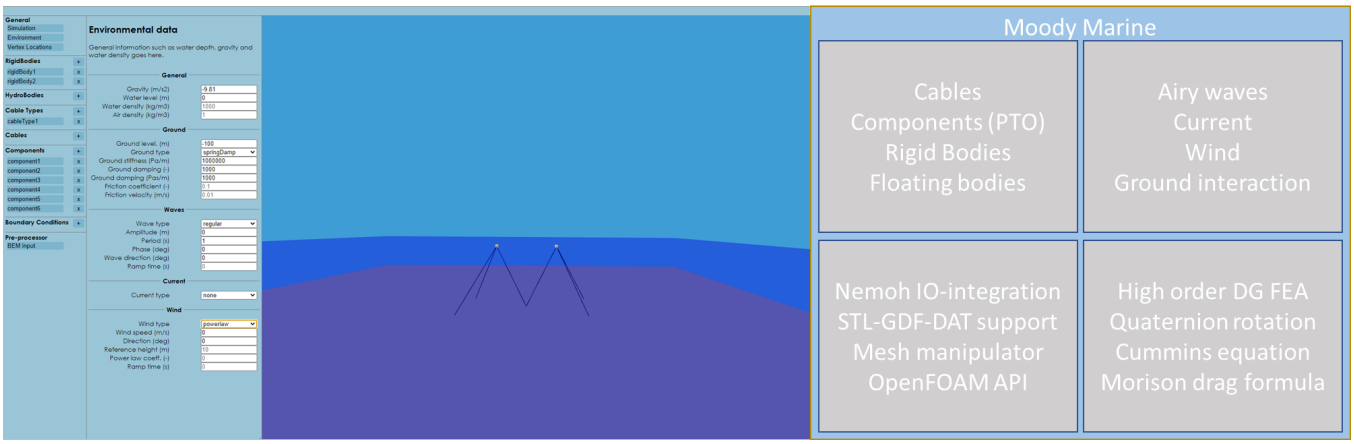

Fig. 1. Screenshot of MoodyMarine with keywords to content.

5) Use the mesh manipulator to cut the mesh at the free surface when at equilibrium position.
6) Specify desired Nemoh data and execute Nemoh's pre-processor and Nemoh.
7) Load Nemoh results and run full time-domain evaluation in MoodyMarine.
8) Post-process the results using either the plotting features in MoodyMarine or export the data and plot using python or matlab.

III. Governing equations

The governing equations of MoodyCore are described below.

A. Wave kinematics

MoodyCore uses the first order velocity potential to describe the incident wave field from one or several wave components. To simplify notation, the following relates to a single regular wave component. The formulation is consistent with the zero-phase convention used in Nemoh. The wave elevation η is

$$\eta = a\cos(k_x x + k_y y - \omega t + \phi) \quad (1)$$
$$= \Re\left(a e^{k_x x + k_y y - \omega t + \phi}\right), \quad (2)$$

with a denoting amplitude, k_x and k_y the wave number components in x and y respectively, ω as the angular frequency, ϕ as the wave phase and t as the time. It relates to a complex incident wave potential Φ_I as

$$\Phi_I = -i\frac{ag}{\omega} Z(\zeta) e^{k_x x + k_y y - \omega t + \phi}, \quad (3)$$

$$Z(\zeta) = \frac{\cosh k(h+\zeta)}{\cosh kh}, , \quad (4)$$

$$\zeta(z,\eta) = h\left(\frac{h+z}{h+\eta} - 1\right) \quad (5)$$

where ζ is the Wheeler stretched vertical coordinate [18]. $Z(\zeta)$ is the depth variation factor, which is evaluated as $e^{k\zeta}$ below the deep water limit defined in moody core as: $k\zeta \leq \pi$.

MoodyCore supports Airy waves as well as first-order irregular waves based on either the Jonswap spectrum or by custom definition on a wave-by-wave mode basis.

B. Floating bodies

MoodyCore uses the following definitions of the first order potential flow forces on a floating body:

F_{rad} Radiation force from the radiation potential Φ_{rad}, realised through the radiation Kernel (also known as the impulse response function) convolution integral with body velocity. Linearised at the initial body position.

F_{df} Diffraction force from the diffraction potential Φ_{df} (sometimes referred to as the scattered potential).

$F_{fk}^{(d)}$ Dynamic Froude-Krylov force from the integral of dynamic pressure in the incident wave potential Φ_I over the wetted body surface.

$F_{fk}^{(s)}$ Static Froude-Krylov force, being the hydrostatic pressure integrated over the wetted body surface.

F_{fk} Total Froude-Krylov force, the sum of static and dynamic Froude-Krylov forces $F_{fk} = F_{fk}^{(s)} + F_{fk}^{(d)}$.

F_{ex} Complex-valued excitation force, $F_{ex} = F_{fk}^{(d)} + F_{df}$

In the fully linear simulation of the Cummins equation, F_{ex} is used to as external wave forcing for any wave amplitude, and the linearized hydrostatic force $F_{fk}^{(s)}$ is transformed into a constant restoring stiffness matrix $\mathbf{C}$ times the body displacement $\vec{x}$. When the nonlinear Froude-Krylov formulation is activated, F_{df} is instead used as linearized external wave force, and the restoring force is evaluated as the total Froude Krylov force $F_{fk} = F_{fk}^{(s)} + F_{fk}^{(d)}$. The total FK force is reported in the restoring force output of the body, and the excitation force output covers only the linearized diffraction force.

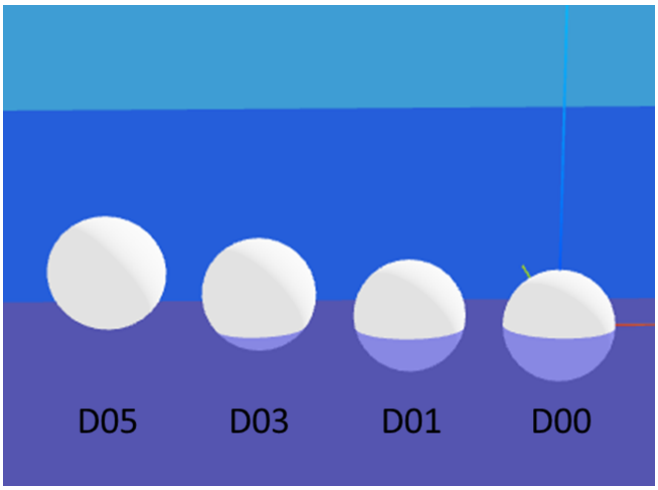

Fig. 2. Heave decay of a sphere. Initial drop heights.

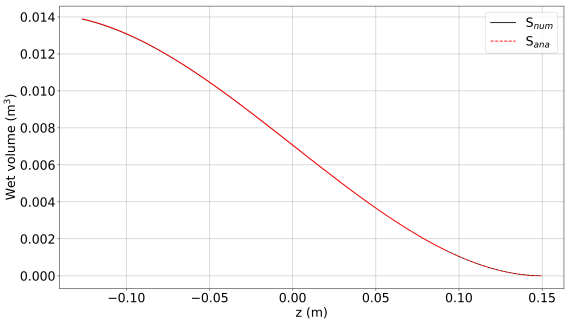

Fig. 3. Heave decay of a sphere. Submerged volume over position.

C. Rigid bodies

Mooring elements such as submerged floaters and sinkers can be modelled using rigid body type objects which are governed by Morrison's equation. The rigid body objects are divided into two categories. One is the simple point mass with an assigned mass and volume but with neglected rotational motion (3DoF object). The other rigid body type also takes the rotation of the body into account (6DoF object). The rotation is modelled using quaternions and the variation of the surrounding fluid is taken into account by integration of the forces on each slice. 6DoF objects will by default use strip theory to to compute the drag forces and moments at each time-step using 7-point numerical quadrature along the symmetry axis. However, the drag force can also be computed in decoupled mode, i.e. to compute rotational drag moment based on the rotation of the body alone, and compute the translational force based on the relative velocity of body and fluid, see [11] for details.

D. Cables

The recent work on floating bodies and GUI originated from the initial work on mooring cable dynamics dating back a decade [19]. MoodyCore implements moorings using the discontinuous Galerkin high-order finite element formulation of [9], with the addition of bending stiffness from [11]. Newtons second law of motion for the mooring lines and dynamic cables is expressed along the curvilinear abscissa $s \in [0, L]$, being the unstretched line coordinate. The balance between inertial, internal and external forces is expressed as:

$$\dot{\vec{\nu}} = \frac{\partial}{\partial s}\left(\vec{T}\right) + \vec{f}_e\,, \tag{6}$$

in which $\vec{\nu} = \gamma_0 \vec{v}$ is the cable momentum per meter (mass per meter γ_0 times velocity $\vec{v}$) and $\vec{T}$ is the internal tension force. $\vec{f}_\mathrm{e}$ represents the external forces acting on a cable segment and can be divided into:

$$\vec{f}_\mathrm{e} = \vec{f}_\mathrm{a} + \vec{f}_\mathrm{b} + \vec{f}_\mathrm{c} + \vec{f}_\mathrm{d}\,, \tag{7}$$

where $\vec{f}_\mathrm{a}$ is the force from the added mass and the Froude–Krylov effect, $\vec{f}_\mathrm{b}$ is the buoyancy force, $\vec{f}_\mathrm{c}$ represents contact forces (ground interaction) and $\vec{f}_\mathrm{d}$ stands for the drag force.

E. Components

Components may be used to represent springs and dampers. They can be used to model mass-less taut moorings, but are also useful for parametrised power-take-off (PTO) models. A PTO can be simulated as a simple spring-damper system of orders P, Q for the stiffness (K) and damping (C) terms respectively,

$$\vec{F}_{pto} = \hat{n} \sum_{i=1}^{P} K_i dL^i + \sum_{j=1}^{Q} C_j \dot{dL}^j\,. \tag{8}$$

However, two-dimensional lookup tables are also supported, enabling a large range of passive attenuated control systems where the control force is interpolated from predefined values on a control surface $F = F(dL, \dot{dL})$.

IV. Verification

A. Sphere decay

A simple decay test using a sphere is used to verify the behaviour of the Cummins equation and nonlinear Froude-Krylov correction. Both were evaluated against experimental data as well as high-fidelity CFD data. The sphere decay originates from the highly accurate experimental campaign of Kramer *et al.* [20], and the high-fidelity CFD data was validated with a very good agreement to said experiments in [21]. The sphere has a density of $\rho_s = 0.5\rho_w$, a mass of $m = 7.00686$ kg and consequently a diameter of $D = 0.3$ m. It is free-floating with a hemispherical displacement. Fig. 2 illustrates how the free-floating sphere (D00) is lifted to three different drop heights (D01, D03 and D05) corresponding to 10%, 30% and 50% of the sphere diameter.

First, the nonlinear restoring force implementation is verified against the analytical result during the D05 drop case in Fig. 3, showing a near perfect fit as the numerical and analytical lines are plotted on top of each other. The mesh used for the nonlinear Froude-Krylov force in this case was very dense (19800 triangles) to miminize truncation errors on the geometry.

Secondly, the results of the heave motion for the D01, D03 and D05 drop cases are shown in Fig. 4 for

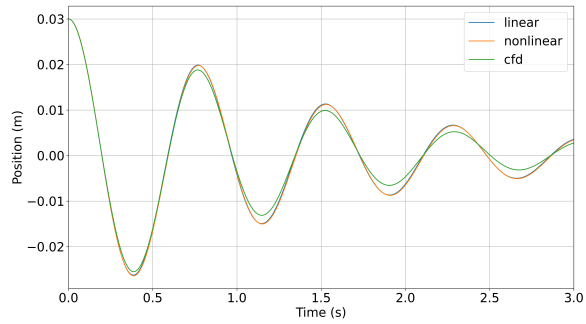

(a)

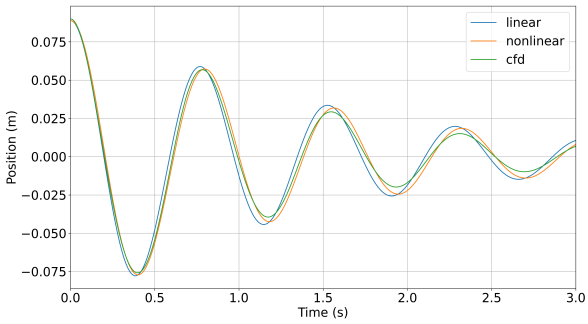

(b)

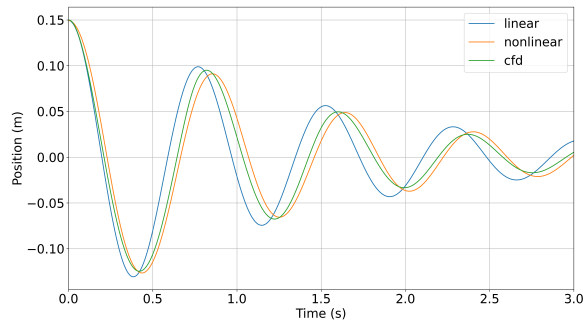

(c)

Fig. 4. Heave decay of a sphere. Drop heights (a) $0.1D$, (b) $= 0.3D$, and (c) $0.5D$.

both linear (lin) and nonlinear (nfk) restoring force approximations. The nonlinear Froude-Krylov correction provides a better phase alignment between CFD and Cummins equation. This is, of course, most clearly seen for the most nonlinear D05 case. These results are well in line with the findings of [20], [22].

Finally, the influence of the resolution, i.e. the number of triangles N of the stl representation, on the performance of the nlfk implementation is examined. Please note that it is only the nlfk part that is affected by the resolution test. All simulations uses the same hydrodynamic coefficients. The influence of N illustrated in Fig. 5 for the D05 case. There are noticeable differences between the two coarsest mesh sizes ($N = 180$ and $N = 760$ triangles), however, the two finer resolutions are clearly adequate to capture the nonlinear restoring force without noticeable loss of accuracy. Of note is that the main errors of the coarser meshes

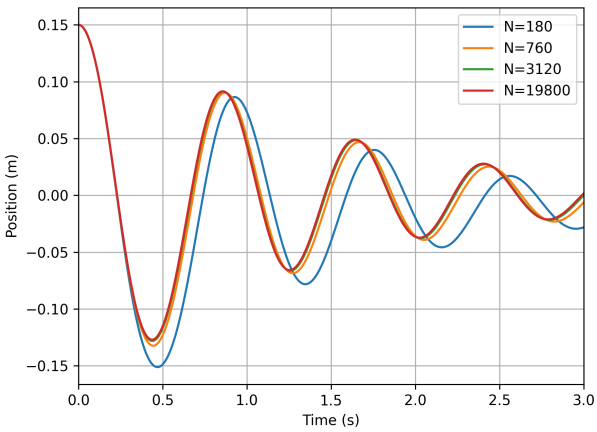

Fig. 5. Heave decay of a sphere. Mesh dependence of nonlinear Froude-Krylov force implementation for the D05 case.

are connected with an underestimated displacement volume, i.e. truncation errors of the volume, which explains why the net position is lower in these cases. The dynamic part of the motion is actually captured with relatively good accuracy for all of the studied meshes.

B. Ellipsoid

Further verification of the nlfk implementation is obtained with a code-to-code comparison between WEC-SIM [3] and MoodyCore. The case is the WEC-SIM demonstration case of a heaving ellipsoid, constrained

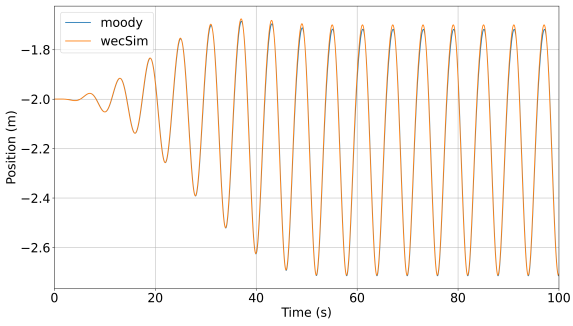

(a)

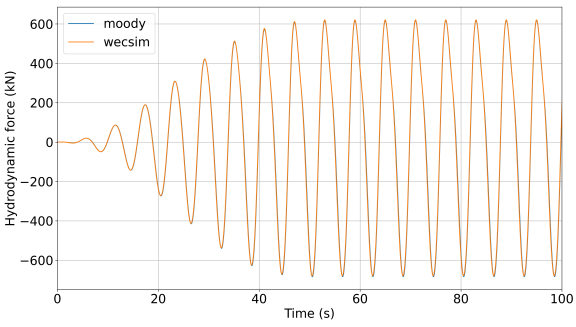

(b)

Fig. 6. Heave decay of an ellipsoid. (a) Heave position, and (b) total force.

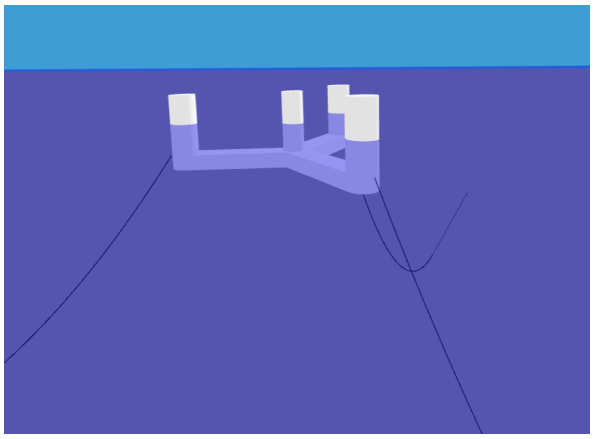

Fig. 7. 3D view of the FOWT.

in other degrees of freedom [23]. The 5 m-major-axis ellipsoid is half-submerged when at rest, $\rho_e = 0.5\rho_w$ with a displacement of 133.4 tonne. The ellipsoid has center of gravity (CoG) at $[0, 0, -2]$ m relative to the waterline, and it is attached with a linear damper of $\nu = 1200$ kNs/m, in turn attached to a fix point 12.5 m down. Figure 6 show the resulting body motion and total force on the ellipse respectively during the analysis of a regular wave $H = 2$ m, $T = 6$ s. Both motion and force compare very well with WEC-Sim results. Drag effects were omitted in this verification.

V. Validation

A. Moored FOWT

A floating offshore wind turbine (FOWT) was the topic of the first floating FOWT comparative study [24]. A slack-moored 1:70 scale model of the UMaine VolturnUS-S semi-submersible platform [25] has been experimentally tested tested in the COAST Laboratory Ocean Basin at the University of Plymouth, UK [26]. However, as the experimental data is not yet freely available we in this study compare to the CFD simulations of the system presented in [27].

The FOWT is shown in Fig. 7. It is made up of equiangularly spaced outer cylinders and a central

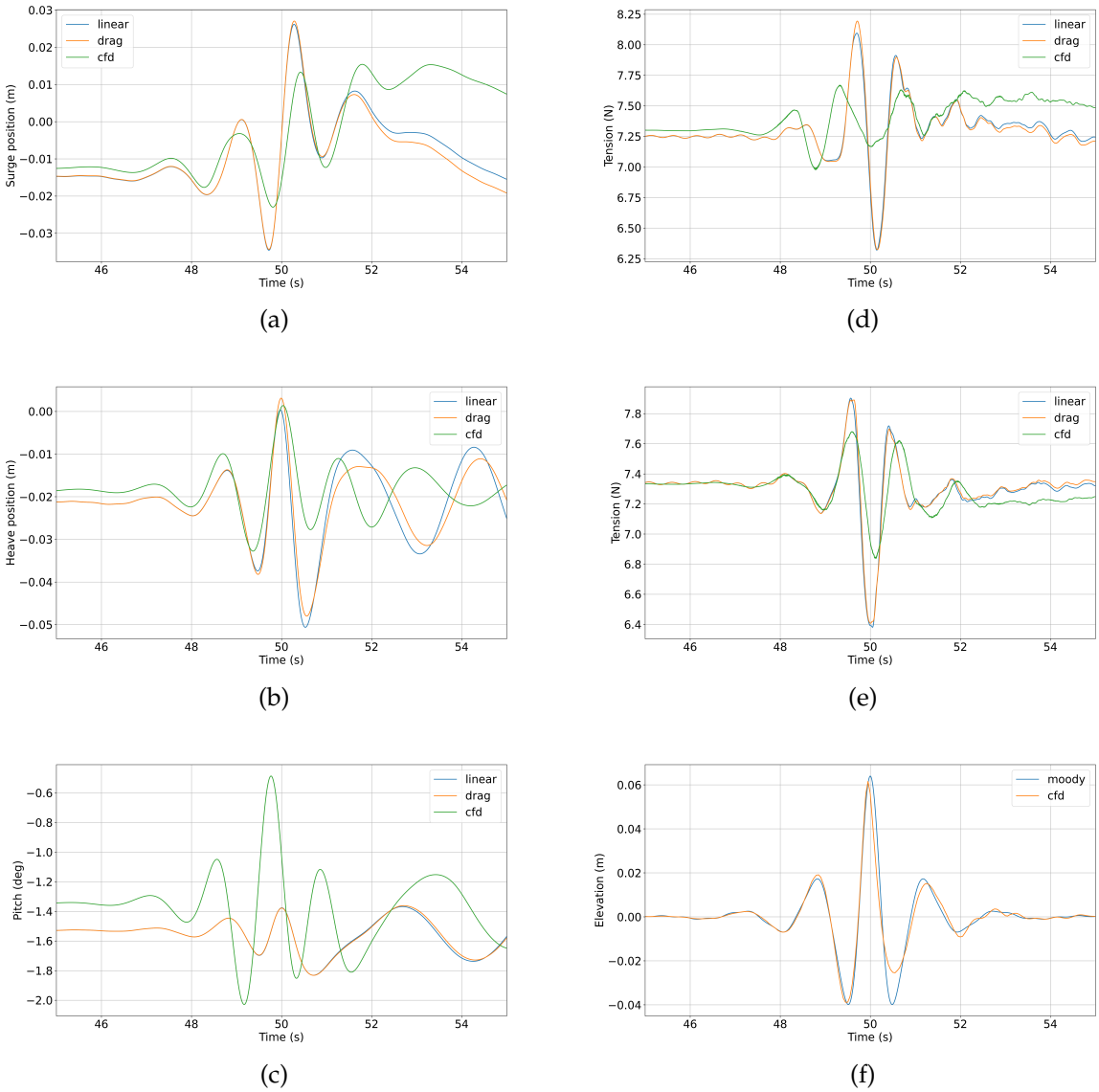

Fig. 8. Results for the benign focused wave case. (a) surge motion, (b) heave motion, (c) pitch motion, (d) tension fore line, (e) tension aft lines, and (f) wave elevation.

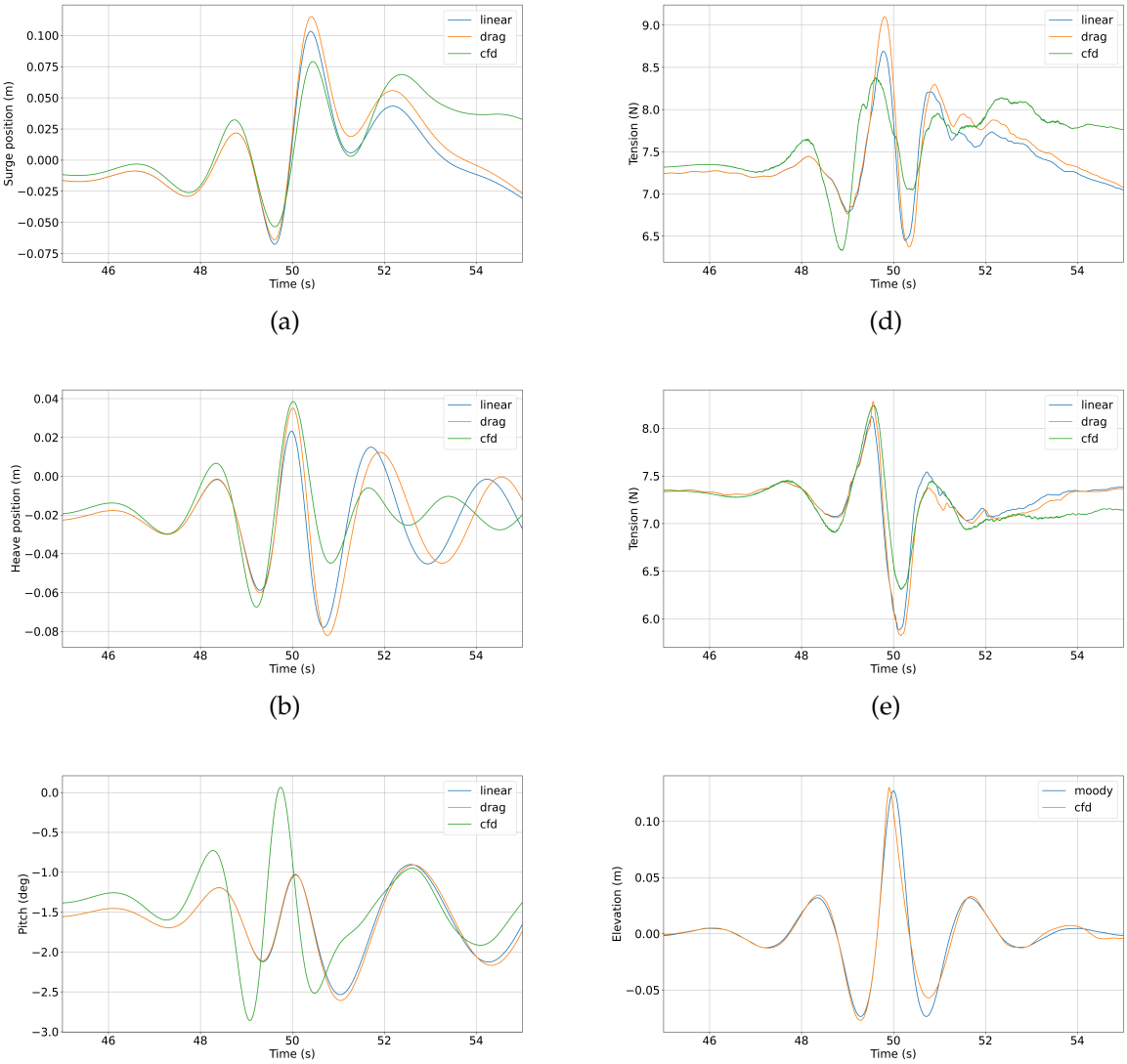

Fig. 9. Results for the harsh focused wave case. (a) surge motion, (b) heave motion, (c) pitch motion, (d) tension fore line, (e) tension aft lines, and (f) wave elevation.

cylinder. The outer and central cylinders are connected by pontoons at the bottom of the cylinders, as well as with braces at the top of the cylinders. A tower with a simplified nacelle-rotor is mounted on the central cylinder. The FOWT is moored with three mooring lines distanced 120 degrees apart: one seaward line in the direction of the waves, and two slightly shorter aft lines. Please note that neither braces nor tower are included in the following study as they are not interacting with the water flow. For all basin, mooring and structure data we refer to [24], [26].

We look here at two focused wave cases. The focused waves are generated using linear dispersive focusing described by the NewWave theory [28] based on a Pierson-Moskowitz spectrum. The benign and harsh wave cases have peak periods $T_p = 1.383$ s and $T_p = 1.938$ s, and crest amplitude $A_{cr} = 0.064$ m $A_{cr} = 0.127$ m, respectively. Figs. 8 and 9 present the results in terms of wave elevation, surge, heave and pitch motion and tensions in the fore and aft mooring lines. Generally, the fit between CFD and MoodyMarine is not perfect, as could be expected for focused waves. The dynamics is captured but there are discrepancies in the amplitudes.

Starting with the benign case we see that there is too little dampening in the LPF surge motion compared to the CFD surge and that the maximum peak in heave is captured accurately but not the following trough. This is partly due to the fact that the analytic wave elevation is symmetric whereas the CFD predicts a shallower second trough. The pitch is not well captured at all, but these are small overall pitch motions. The exaggerated surge motion and the poor match of the pitch is carried over to the mooring line tensions, where especially the minimum tension is under predicted by MoodyMarine.

For the harsh wave case the fit is slightly better. We see that the surge and heave response more closely resemble the CFD data, whereas the pitch is still off. However, the tension time-series show a much improved match compared to the benign case. This is judged to be due to the better prediction of the surge motion. Finally, for these cases adding Morrison drag

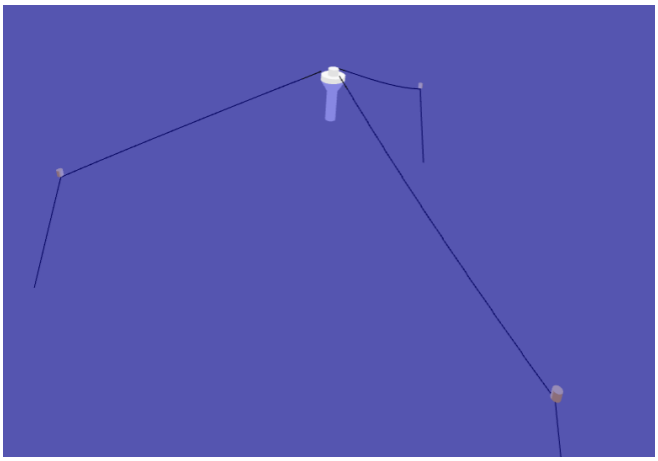

Fig. 10. 3D view of the Waves4Power WEC.

to the FOWT gave little effect as can be seen from Figs. 8 and 9. The drag force coefficients were estimated from DNV [29] using $CD = 1.9$ applied to the bottom area of the float for the vertical motion, and $CD = 1.0$ for the horizontal motion, combined with the projected area of the four columns.

B. Waves4Power self-reacting WEC

In the final validation case we consider a single WEC device in full-scale, based on the self-reacting point-absorber Waves4Power buoy [30]. The Waves4Power system consists of an axi-symmetric WEC, in which the PTO reacts against a heave plate inside a tube. The device is moored with three hybrid mooring legs consisting of a lower and an upper polyester rope, attached to an intermediate submerged cylindrical buoy, see Fig. 10

This device has been investigated in detail by [31] using linear potential flow as well as by CFD simulations in [10], [15]. In the following we will compare to the CFD simulations [15]. For all environmental, mooring and structure data we refer to [15], [31].

We consider here the case of a linear incident regular wave with $T = 7$ s and $H = 2$ m. The water depth is 90 m. In the simulations the WEC is modelled as a radiation-diffraction body, the tube is simplified as being closed, and the PTO is given by a linear damper working in body coordinate heave. The submerged buoys are treated as 6DoF Morrison bodies with $CM = 0.66$ and $CD = 0.73$, obtained from comparison to CFD simulations in [11].

The WEC motion is presented in Fig. 11. The heave amplitude is slightly larger than predicted by CFD. The surge offset are clearly visible in both the LPF and CFD results. The surge amplitude is just like the heave amplitude slightly larger for the LPF compared to CFD. These differences are most likely due to under-resolution of the CFD simulation. The pitch amplitude is well captured with only minor differences between MoodyMarine and CFD. In all there is a general good agreement between MoodyMarine and the CFD solutions, as could be expected for this rather linear test case.

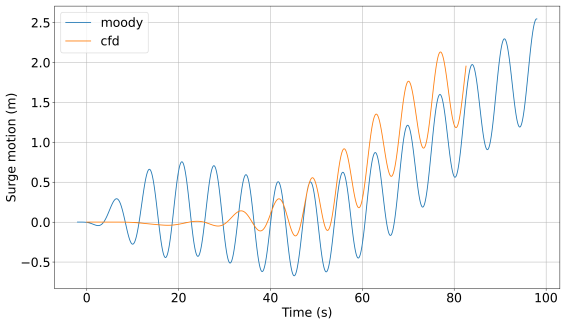

(a)

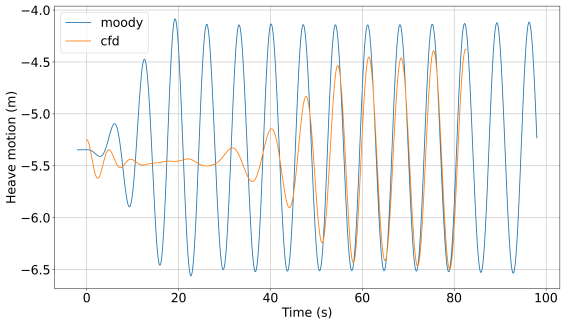

(b)

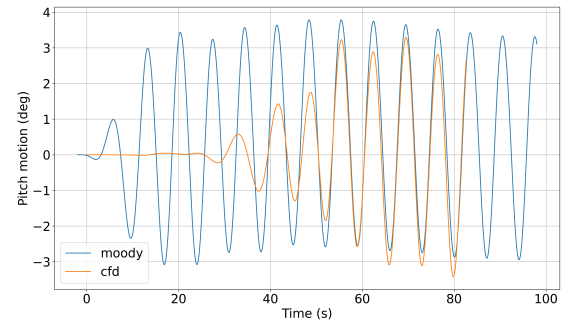

(c)

Fig. 11. Motion of the Waves4Power WEC: (a) surge motion, (b) heave motion and, (c) pitch motion.

VI. Concluding Remarks

We have presented the linear potential flow solver MoodyMarine. MoodyMarine is a GUI layer on top of the MoodyCore C++ implementation for time-domain modelling of mooring lines and floating bodies in waves. MoodyMarine is distributed as freeware and can be downloaded from **`www.moodymarine.se`**.

The individual components of MoodyCore have been validated in previous publications. In this work we showed a verification of the newly developed feature of nonlinear Froude-Krylov force. Decay tests of a sphere and an ellipsoid yielded results in line with other weakly nonlinear codes as well as CFD models. The use of MoodyMarine for more complex MRE systems were illustrated by a slack-moored FOWT and a point-absorber with hybrid mooring. It was shown that, within the LPF underlying assumptions, MoodyMarine gave reasonable results compared to

CFD simulations.

ACKNOWLEDGEMENT

We gratefully acknowledge that the computations were performed on resources at the National Supercomputer Centre provided by the National Academic Infrastructure for Supercomputing in Sweden (NAISS).

REFERENCES

[1] "https://www.orcina.com/orcaflex/," 2023.
[2] "https://dsaocean.com/proteusds/," 2023.
[3] K. Ruehl, D. Ogden, Y.-H. Yu, A. Keester, N. Tom, D. Forbush, J. Leon, J. Grasberger, and S. Husain, "Wec-sim v5.0.1," 2022. [Online]. Available: https://zenodo.org/badge/latestdoi/20451353
[4] H. Bingham and R. Read, "DTUMotionSimulator: a Matlab package for simulating linear or weakly nonlinear response of a floating structure to ocean waves," 2022. [Online]. Available: https://gitlab.gbar.dtu.dk/oceanwave3d/DTUMotionSimulator
[5] G. Giorgi, G. Bracco, and G. Mattiazzo, "NLFK4ALL: An open-source demonstration toolbox for computationally efficient nonlinear Froude-Krylov force calculations," in *Proceedings of the 14th World Congress on Computational Mechanics (WCCM) ECCOMAS Congress 2020*, Paris, France, 2020.
[6] "https://react.dev/learn," 2023.
[7] "https://threejs.org," 2023.
[8] "https://www.electronjs.org," 2023.
[9] J. Palm, C. Eskilsson, and L. Bergdahl, "An *hp*-adaptive discontinuous Galerkin method for modelling snap loads in mooring cables," *Ocean Engineering*, vol. 144, pp. 266–276, 2017.
[10] J. Palm and C. Eskilsson, "Mooring systems with submerged buoys: influence of floater geometry and model fidelity," *App. Ocean Res.*, vol. 102, no. 102302, 2020.
[11] ——, "Influence of bending stiffness on snap loads in marine cables: A study using a high-order discontinuous Galerkin method," *Journal for Marine Science and Engineering*, vol. 8, no. 10, p. 795, 2020.
[12] ——, "On end-stops and snap loads for taut-moored wave energy converters," in *Proceedings of the 14th European Wave and Tidal Energy Conference (EWTEC2021)*, Plymouth, UK, 2021.
[13] ——, "Moodycore v3.0 manual," Tech. Rep., 2023.
[14] J. Palm, C. Eskilsson, G. M. Paredes, and L. Bergdahl, "Coupled mooring analysis for floating wave energy converters using CFD: Formulation and validation," *Int. J. Mar. Energy*, vol. 16, pp. 83–99, 2016.
[15] C. Eskilsson and J. Palm, "High-fidelity modelling of moored marine structures: multi-component simulations and fluid-mooring coupling," *Journal of Ocean Engineering and Marine Energy*, vol. 8, no. 4, pp. 513–526, 2022.
[16] C. Eskilsson, J. Palm, P. Johannesson, and G. Paredes, "Sensitivity analysis of extreme loads acting on a point-absorbing wave energy converter," *International Marine Energy Journal*, vol. 5, no. 1, pp. 91–101, 2022.
[17] R. Kurnia and G. Ducrozet, "NEMOH v3.0 User Manual," Tech. Rep., 2022.
[18] J. Wheeler, "Method for calculating forces produced by irregular waves," *Journal of Petroleum Technology*, vol. 22, no. 3, pp. 359–367, 1970.
[19] J. Palm, G. Paredes, C. Eskilsson, F. Taveira-Pinto, and L. Bergdahl, "Simulation of mooring cable dynamics using a discontinuous Galerkin method," in *Proceedings of the V International Conference on Computational Methods in Marine Engineering (MARINE 2013)*, Hamburg, Germany, 2013.
[20] M. B. Kramer, J. Andersen, S. Thomas, F. B. Bendixen, H. Bingham, R. Read, N. Holk, E. Ransley, S. Brown, Y.-H. Yu, T. T. Tran, J. Davidson, C. Horvath, C.-E. Janson, K. Nielsen, and C. Eskilsson, "Highly accurate experimental heave decay tests with a floating sphere: A public benchmark dataset for model validation of fluid–structure interaction," *Energies*, vol. 14, no. 2, p. 269, 2021. [Online]. Available: https://www.mdpi.com/1996-1073/14/2/269
[21] C. Eskilsson, A. Shiri, and E. Katsidoniotakis, "Solution verification of WECs: comparison of methods to estimate numerical uncertainties in the OES wave energy modelling task," in *Proceedings of the 15th European Wave and Tidal Energy Conference*, Bilbao, Spain, 2023.
[22] F. Wendt, K. Nielsen, Y.-H. Yu, H. Bingham, C. Eskilsson, M. Kramer, A. Babarit, T. Bunnik, R. Costello, S. Crowley, B. Gendron, G. Giorgi, S. Giorgi, S. Girardin, D. Greaves, P. Heras, J. Hoffman, H. Islam, K.-R. Jakobsen, C.-E. Janson, J. Jansson, H. Y. Kim, J.-S. Kim, K.-H. Kim, A. Kurniawan, M. Leoni, T. Mathai, B.-W. Nam, S. Park, K. Rajagopalan, E. Ransley, R. Read, J. V. Ringwood, J. M. Rodrigues, B. Rosenthal, A. Roy, K. Ruehl, P. Schofield, W. Sheng, A. Shiri, S. Thomas, I. Touzon, and I. Yasutaka, "Ocean energy systems wave energy modelling task: Modelling, verification and validation of wave energy converters," *Journal of Marine Science and Engineering*, vol. 7, no. 11, 2019. [Online]. Available: https://www.mdpi.com/2077-1312/7/11/379
[23] M. Lawson, Y.-H. Yu, A. Nelessen, K. Ruehl, and C. Michelen, "Implementing nonlinear buoyancy and excitation forces in the WEC-Sim wave energy converter modeling tool," in *Proceedings from the 33rd International Conference on Ocean, Offshore and Arctic Engineering (OMAE 2014)*, San Francisco, US, 2014.
[24] "https://www.ccp-wsi.ac.uk/data_repository/test_cases/test_case_015," 2022.
[25] C. Allen, A. Viscelli, H. Dagher, A. Goupee, E. Gaertner, N. Abbas, M. Hall, and G. Barter, "Definition of the UMaine VolturnUS-S reference platform developed for the IEA wind 15-megawatt offshore reference wind turbine," https://www.osti.gov/biblio/1660012, 2020.
[26] E. Ransley, S. Brown, E. Edwards, T. Tosdevin, K. Monk, A. Reynolds, D. Greaves, and M. Hann, "Hydrodynamic response of a floating offshore wind turbine (1st fowt comparative study dataset)," PEARL Research Repository https://doi.org/10.24382/71J2-3385, 2022.
[27] C. Eskilsson, G. V. Fernandez, J. Andersen, and J. Palm, "Hydrodynamic simulations of a FOWT platform (1st FOWT comparative study) using openfoam coupled to moodycore," in *Proceedings of the 15th European Wave and Tidal Energy Conference*, Ottawa, Canada, 2023.
[28] P. Tromans, A. Anaturk, and A. Hagemeijer, "A new model for the kinematics of large ocean waves-application as a design wave," in *Proceedings from the 1st International Offshore and Polar Engineering Conference (ISOPE)*, Edinburgh, UK, 1991, p. 64–71.
[29] D. N. Veritas, "Dnv-rp-c205: Environmental conditions and environmental loads," Tech. Rep., 2014.
[30] Waves4Power AB, "https://www.waves4power.com," 2022.
[31] S.-H. Yang, "Analysis of the fatigue characteristics of mooring lines and power cables for floating wave energy converters," Ph.D. dissertation, Chalmers University of Technology, 2018.